PAPER

Check for updates

Impact of drying/wetting conditions on the binding characteristics of Cu(II) and Cd(II) with sediment dissolved organic matter

Mi Zhou,[a] Zhongwu Li, [ID] *[ab] Mei Huang,[b] Xiang Ding,[b] Jiajun Wen[b] and Lei Wang[a]

The biogeochemical processing of dissolved organic matter (DOM) in bottomland sediment under drying/wetting conditions regulates the environmental behavior of heavy metals. Although moisture is a critical factor, the structural characteristics of DOM and its reactivity with heavy metals under drying/wetting conditions are not well known. Herein, the response of DOM to drying/wetting conditions and its influence on the binding of Cu(II) and Cd(II) onto DOM were clarified *via* various multi-spectroscopic techniques. Ultraviolet-visible spectra (UV-Vis) showed that higher aromatic, hydrophobic, and molecular weight fractions were observed in sediment DOM under drying conditions than those under wetting conditions. The binding abilities for Cd(II) with DOM under drying/wetting conditions are lower than those for Cu(II). The stability constants between Cu(II) and DOM were found to decrease under drying/wetting conditions; however, the binding capacities for Cu(II) increased, especially under wetting conditions. Two-dimensional correlation spectroscopy based on Fourier-transform infrared (FTIR) and synchronous fluorescence spectra (SFS) showed that Cu(II) and Cd(II) have different binding sequences and binding sites and that Cu(II) has more binding sites under drying and wetting conditions; however, Cd(II) shows the opposite behavior. These results clearly demonstrate that the binding of sediment DOM with Cu(II) is more prevalent and stable compared with Cd(II) under drying and wetting conditions. Because of its relatively low binding capacity and binding stability, Cd(II) can exhibit a high environmental hazard for migration and transformation with DOM due to water flow under wetting conditions. This study helps reveal the impact of drying/wetting conditions on the environmental behavior of heavy metals in bottomland wetlands.

1 Introduction

The bottomland area of a lake is important, as it serves as the fundamental structure of lake ecosystems.[1] Bottomland sediment can significantly influence water quality and the ecological functions of lake ecosystems. However, with the development of industrialization and urbanization, bottomland areas have become vulnerable to the prevalence of heavy metals, such as Cu and Cd.[2,3] Dissolved organic matter (DOM), which serves as the active fraction of sediment, plays a fundamental role in element cycling and energy circulation in aquatic ecosystems.[1,4] DOM is known to form strong complexes with heavy metals, and DOM–metal complexes, as one factor, govern the distribution, toxicity, bioavailability, and ultimate fate of heavy metals in the environment.[5] Therefore, it is necessary to understand the effect of sediment DOM on the environmental behavior of heavy metals.

The alternation of drying and wetting characteristics is a typical feature of a bottomland area because of the periodic rise and fall of the water level. Drying/wetting alternation can result in the sediment undergoing aerobic/anaerobic physical, chemical, and biological changes, which affect the composition and structure of DOM.[6] For example, aromatic constituents can be selectively preserved under wetting conditions; meanwhile, the aromaticity, hydrophobicity and molecular weight of DOM can be gradually decreased under wet conditions.[7] Interestingly, studies have shown that highly aromatic substances exhibit strong stability when combined with Cu(II).[8–10] Based on these studies, we speculated that the differences in the composition characteristics of DOM under different environmental conditions affects the binding behavior of DOM with heavy metals. To date, many previous studies have focused on the concentration and distribution of heavy metals in bottomland sediment and the effect of drying/wetting conditions on the release of heavy metals.[11,12] In addition, the composition and structural characteristics of DOM from different origins have also been deeply investigated.[13] However, few studies have attempted to explore the characteristics of DOM in sediments under alternating drying/wetting conditions or the effects of moisture on the

aCollege of Resource and Environment Science, Hunan Normal University, Changsha, 410081, PR China. E-mail: lizw@hnu.edu.cn

bCollege of Environmental Science and Engineering, Hunan University, Key Laboratory of Environmental Biology and Pollution Control (Hunan University), Ministry of Education, Changsha, Hunan 410082, PR China

binding of DOM with heavy metals. Hence, it is of great significance to study the binding characteristics of DOM with heavy metals in bottomland sediments under drying/wetting conditions and to guide the prevention of heavy metals in wetlands.

Metal ions can result in fluorescence quenching for DOM, which serves as an effective indicator for the analysis of the binding properties of DOM with heavy metals.[14] Currently, techniques used for characterizing organic matter include ultraviolet-visible spectroscopy (UV-Vis), Fourier-transform infrared spectroscopy (FTIR), Fourier-transform ion cyclotron resonance mass spectrometry, chromatography, and synchronous fluorescence spectra (SFS).[15,16] Owing to the complexity of the components of sediment DOM, it is difficult to evaluate the composition and interaction of substances with only one spectral technique.[14,17] Therefore, three spectral techniques, namely, UV-Vis, FTIR, and SFS, were used in this study. The objectives of this work were as follows: (a) to determine and discuss the difference in the structural characteristics of sediment DOM under drying and wetting conditions using spectral analysis combined with a parallel factor analysis (PARAFAC) model; (b) to comparatively analyze the binding capacities, stability constants, and binding site sequence for Cu(II) and Cd(II) with sediment DOM under drying/wetting conditions using two-dimensional correlation spectroscopy analysis combined with FTIR (2D-FTIR-COS) and SF spectra (2D-SFS-COS); and (c) to reveal the impact of drying/wetting conditions on the binding of DOM with heavy metals.

2 Materials and methods

2.1 Incubation experiments of sediment

The sediment samples used in this study were collected from Junshan Island in East Dongting Lake, Hunan Province, China (29° 26′ 22″ N, 112° 59′ 50″ E) in March 2019. The collected sediments were air-dried, ground (2 mm) and then further treated with incubation experiments. Next, 30 kg of sediment was divided into 6 aliquots of 5 kg each into plexiglass columns with a length of 120 cm and a diameter of 15 cm. Then, sediment moisture was adjusted to 70% of water holding capacity (WHC) and incubated in darkness at 25 °C for 7 d in order to activate the existing microbial communities according to Muhammad et al.[18] To simulate the environmental conditions of bottomland sediment, samples were divided into two batches (with three replicates): one batch with drying treatment (no water was added during the experiment after incubation) and another batch with continuous wetting treatment (30–40 cm water layer over the surface sediment). The sediment samples were incubated for a total of 90 d. The sediment from the 15 cm diameter columns was divided equally into 6 spots. Then, 150 g of sediment was removed from one spot in each column after gently stripping the surface sediment with a long-handled spoon at 0 days, 7 days, 15 days, 30 days, 60 days and 90 days.

2.2 Water-extractable DOM

All the incubated samples were air-dried, ground to pass through a 60-mesh sieve, and then used for the extraction of

DOM, as described by Li et al.[7] and Yu et al.[19] Sediment was extracted with ultrapure Milli-Q water using a solid/liquid ratio of 1/5 (w/v) and shaking for 24 h at 220 rpm and 25 °C. After centrifuging at 4000 rpm for 30 min, the supernatant was filtered through a 0.45 μm membrane. The filtrates were then stored at 4 °C until further analysis. The DOM concentration in the sediment was expressed as the dissolved organic carbon (DOC) concentration in accordance with Jiang et al.[20] The DOC was measured by a total organic carbon (TOC) analyzer (TOC-V CPH, Shimadzu, Japan).

2.3 Spectral experiments

The fluorescence excitation–emission matrix (EEM) for the DOM was obtained by using a fluorescence spectrometer (F-7000, Hitachi, Japan). EEM spectra were gathered by measuring the fluorescence intensity across excitation wavelengths in the range 200–500 nm (sampling interval 5 nm) and emission wavelengths in the range 250–600 nm (sampling interval 2 nm) with a scan rate of 2400 nm min^{-1}. The slit widths for both emission and excitation were set as 5 nm. For the blank scans, Milli-Q water was applied for every 10 analysis samples. Synchronous fluorescence spectra were recorded with the same fluorescence spectrometer used for the EEM spectra at a scan rate of 240 nm min^{-1} with excitation and emission slit sizes of 5 nm. The excitation wavelengths were scanned from 250 nm to 500 nm (every 0.6 nm) with a constant offset of $\Delta\lambda = 60$ nm, which can provide a higher fluorescence intensity and better resolution.[5]

For UV-Vis analysis, all the DOM samples were measured at wavelengths ranging from 800 nm to 190 nm using a Shimadzu UV-Vis spectrophotometer with a 1 cm quartz cuvette (UV-2550, Shimadzu, Japan). The aromaticity, hydrophobicity and molecular weight of DOM were expressed as SUVA$_{254}$, SUVA$_{260}$ and S_R, respectively.[7] SUVA$_{254}$ and SUVA$_{260}$ were calculated as the ratio of the UV absorption at 254 nm and 260 nm to the DOC concentration, respectively.[21,22] The slope ratio (S_R) is a dimensionless parameter, which was calculated as the ratio of the slope of the shorter wavelength region (275–295 nm) to that of the longer wavelength region (350–400 nm).[22]

2.4 Quenching titration experiment

Quenching titration experiments were conducted to measure the complexation characteristics of DOM with Cu(II) or Cd(II). The DOM solution used in the quenching titration was derived from samples incubated at 0 days and 90 days. Before titration, the DOC concentration of the DOM solution was diluted to 6 mg C L^{-1}, to minimize the inner filtering effects.[3] Metal titration was performed by adding CuCl$_2$ and CdCl$_2$ (0.02 mol L^{-1} or 0.1 mol L^{-1}) to 35 mL of DOM solution in 100 mL brown sealed vials to generate a series of samples containing Cu(II) and Cd(II) concentrations ranging from 0 μmol L^{-1} to 100 μmol L^{-1}. The pH of the titrated solutions was maintained at 6.0 to avoid precipitation.[23] To reduce the concentration effect as much as possible, the volume of the added solution was less than 5% of the total volume. All the titrated solutions were shaken for 24 h at 25 °C in a dark environment to ensure coordination

equilibrium. Afterwards, a part of the solution was analyzed by fluorescence spectroscopy and synchronous fluorescence spectroscopy, while the remainder of the solution was freeze-dried for FTIR analysis. FTIR spectra over the wavenumber range from 4000 to 400 cm^{-1} were generated using a mixture (KBr to DOM ratio of 1/100) and a Shimadzu Spectrum One FTIR spectrometer (Shimadzu, Japan).

2.5 Complexation modeling

A non-linear model developed by Ryan and Weber was used to determine the complexation parameters for the DOM and heavy metals.[24] According to the Ryan–Weber model, DOM and heavy metal complexes can be formed with metal ion to fluorescent ligands or binding sites ratio of 1 : 1. The Ryan–Weber model was applied to calculate the fluorescent complex ratios and conditional stability constants between Cu(II) and Cd(II), along with the fluorescent components identified by the EEM. The Ryan–Weber equation is expressed as follows eqn (1):

$$I = I_0 + (I_{ML} + I_0)\left(\frac{1}{2K_M C_L}\right)\left(1 + K_M \right.$$
$$\left. + \sqrt{(1 + K_M C_L + K_M C_M)^2 - 4K_M{}^2 C_L C_M}\right) \quad (1)$$

The fluorescent complex ratio (f) is the fraction of the initial fluorescence that corresponds to the binding and is determined using eqn (2):

$$f = \frac{I_0 - I_{ML}}{I_0} \times 100\% \quad (2)$$

where I_0 and I represent the intensities of the fluorescent components identified initially and the metal concentration (C_M), respectively. I_{ML} is the intensity at which the fluorescence intensity does not change with any additional increase in metal concentration. C_L and K_M can be represented as the total ligand concentration and conditional stability constant, respectively. Nonlinear fitting was conducted to estimate I_{ML}, K_M, and C_L using nonlinear regression analysis.

2.6 Chemometric analysis

Prior to PARAFAC modeling, the Raman and Rayleigh scatterers were removed, and the fluorescence spectra were calibrated by normalization to the integrated water Raman scattering band (Ex = 350 nm), based on the protocol of Bahram *et al.*[25] PARAFAC analysis was fitted and validated using the DOM Fluor toolbox (http://www.models.life.ku.dk/) in MATLAB R2012b (Mathworks, Natick, MA), following the procedures described by Stedmon and Bro.[26]

Prior to a 2DCOS analysis, synchronous fluorescence spectra and the FTIR spectra were baseline-corrected and denoised by smoothing. 2DCOS analysis was produced using "2D shige" software (Kwansei Gakuin University, Japan). Information for the algorithm adopted in the software has been described by Noda and Ozaki[27] and can be found in previous studies.[9,28]

2.7 Statistical analysis

Statistical analyses were conducted using SPSS 22.0 software. DOC, SUVA$_{254}$, SUVA$_{260}$, and S_R were analyzed using one-way analysis of variance (ANOVA), and the significance levels, which were reported as significant ($p < 0.05$) and non-significant ($p > 0.05$), were determined using a LSD t-test. All graphs were plotted using Origin 2018.

3 Results and discussion

3.1 The properties and fluorescence components of DOM under drying/wetting conditions

Under both drying and wetting conditions, the DOC content showed a generally decreasing trend during the incubation period (Fig. 1a), with values ranging from 10.9 mg L^{-1} to 31.6 mg L^{-1} and 17.4 mg L^{-1} to 38.2 mg L^{-1} for drying and wetting groups, respectively. After 30 d of incubation, a significant decreasing trend for DOC was observed (Fig. 1a, $p < 0.05$), which can be ascribed to the consumption of microorganisms according to Li *et al.*,[7] Tsai *et al.*[29] and Hur *et al.*[30] In addition, the DOC values under wetting conditions were significantly higher than those obtained under drying conditions ($p < 0.05$).

The SUVA$_{254}$ and SUVA$_{260}$ values first increased and then decreased for the drying group, indicating an initial rise and then decline in aromaticity and hydrophobicity in the sediment under drying conditions (Fig. 1b). Also, significantly high values were exhibited at 15 d ($p < 0.05$; 6.63 and 6.37 L mg C^{-1} m^{-1}, respectively), indicating that the aromaticity and hydrophobicity of DOM was the highest at 15 d. However, there was no significant difference in the wetting group. S_R is an index that is inversely proportional to the molecular weight of DOM.[22] The S_R value continuously decreased with time in the drying group, suggesting that the molecular weight of DOM increased during incubation. The S_R value initially decreased and then increased, ultimately gradually stabilizing in the wetting group (Fig. 1d). This indicated that the molecular weight of DOM was high in the early stage and low in the latter stage. The aromaticity, hydrophobicity, and molecular weight of DOM under drying conditions was higher than that under wetting conditions, which might be attributed to the partial decomposition of organic matter and plant residue by aerobic microorganisms and the production of more small organic compounds by biotic aging under aerobic conditions.[31] However, the values of SUVA$_{254}$, SUVA$_{260}$, and S_R showed no significant difference in the sediment of the wetting group ($p > 0.05$). One reason for this might be that under a low oxygen environment, the biomass and activity of microorganisms was limited; another possible reason is that higher levels of aromatic and hydrophobic components may be released into the overlying water,[32] leading to slight variation in the aromaticity and hydrophobicity of DOM in the wetting group. These results are inconsistent with those obtained by Li *et al.*,[7] which may be ascribed to the different properties of river sediment and paddy soil.

To further illustrate the component characteristics of DOM, EEM-PARAFAC was applied to characterize and identify the DOM components. The characteristics of each component in
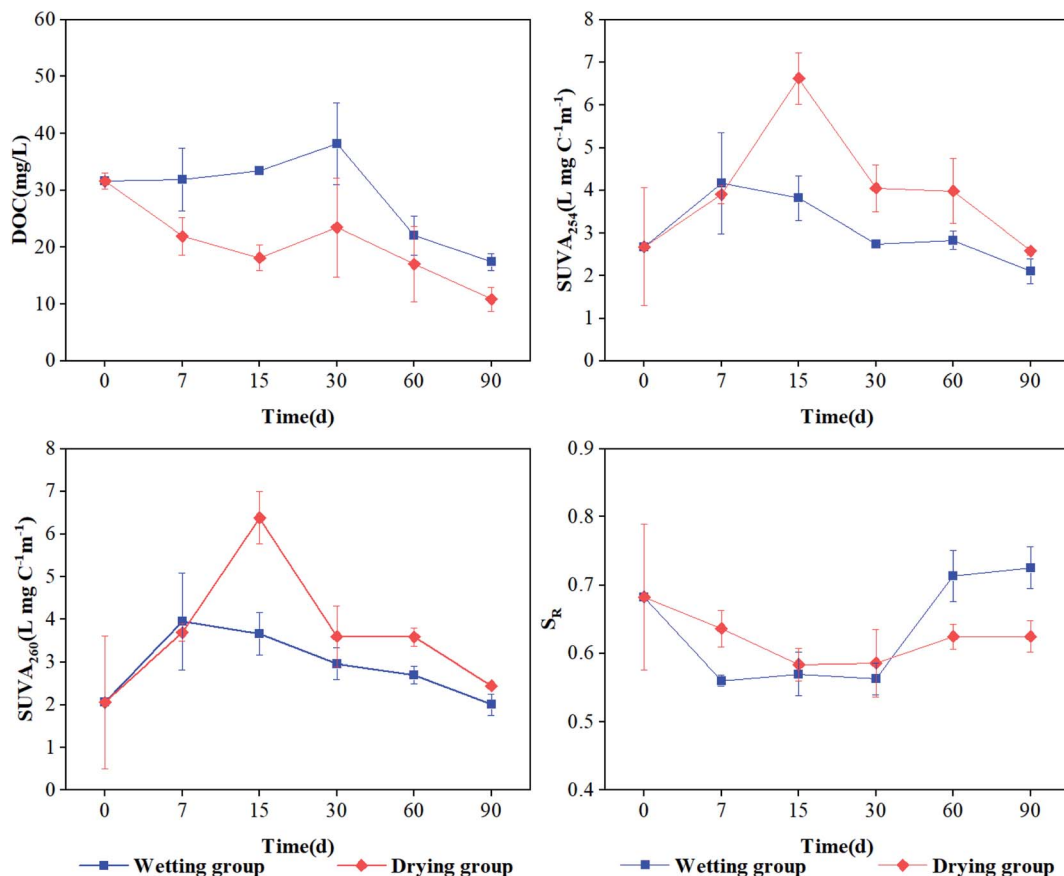
Fig. 1 DOC and optical characteristics of DOM derived from sediment under drying and wetting conditions throughout the incubations. Error bars represent standard deviations ($n = 3$).

the present study and their comparison with previous studies are displayed in Table 1. The results showed that one humic-like substance (C1) and two protein-like substances (C2, C3) were identified in different incubation stages (Fig. 2). C1 component (Ex/Em = 250/428 nm) is a terrestrial humic-like component, similar to the DOM component investigated in Dongting Lake sediment of Li et al. (Region IV).[33] This component has also been found in biochar (C4 (ref. 34)), macrophyte (C1 (ref. 1) and C1 (ref. 10)), and aquatic systems (C3 (ref. 3) and C1 (ref. 32)), which are expected to consist of compounds with abundant aromatic structures and a high molecular weight.[3,9,34–37] The C2 component exhibits excitation maxima in the wavelength range of 220–230 nm and an emission maximum at 300 nm, and is classified as a tyrosine-like substance, similar to the DOM

component investigated in coastal environments (C7 (ref. 38)), Cryoconite (Peak B[39]) and compost (C4 (ref. 40) and C4 (ref. 9)). A tyrosine-like substance is formed by biodegradable tyrosine, which represents the fluorescent group related to the aromatic protein structure produced by microbial degradation.[20] The C3 component shows a strong fluorescence at the excitation/emission wavelengths in the wavelength ranges of 220–230/338 nm and 270–290/338 nm, which is ascribed to a tryptophan-like substance, as also found in the research of Yamashita et al. (C4 (ref. 38)) and He et al. (C3 (ref. 40)) tryptophan is considered as a dissolved microbial metabolite, produced by the degradation and metabolism of microorganisms and bacteria,[39] which is similar to a protein-like fluorescent compound observed previously.[10,35,41]

Table 1 Characteristics of the three components identified in the present study compared with those previously identified

| Present study		Previous studies	
Components	Ex/Em (nm)	Fluorescent substance types[54] (wavelength region)	References
C1	250/428	Humic-like substance (Ex/Em = 240–270/370–480)	Region IV,[33] C1,[1] C4,[34] C1,[10] C1 (ref. 32)
C2	220–230/300	Tyrosine-like substance (Ex/Em = 220–230/300–320)	Region I,[33] Peak B,[39] C4,[9] C4 (ref. 40)
C3	220–230 (270–290)/338	Tryptophan-like substance (Ex/Em = 270–290/320–350)	C4,[38] C3,[40] C5 (ref. 41)
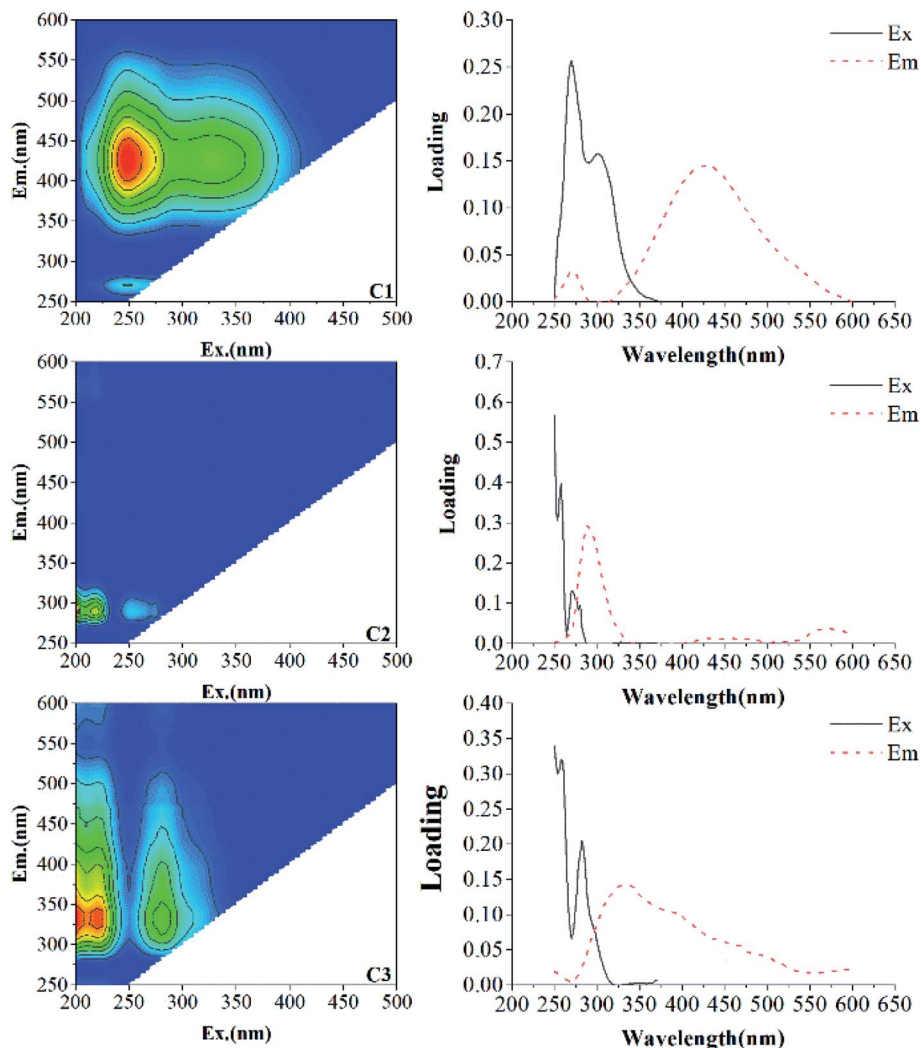
Fig. 2 The excitation–emission matrix (EEM) heatplots of the three fluorescent components (C1: humic-like component; C2: tryptophan-like component; C3: tyrosine-like component) identified by parallel factor analysis (PARAFAC).

3.2 Interactions of PARAFAC-derived components with Cu(II) and Cd(II)

PARAFAC and complexation models were used to identify the effects of both drying and wetting on the Cu(II) and Cd(II) binding ability and stability of DOM. The results showed the variations in the fluorescent intensities for the three PARAFAC-derived components under both drying and wetting conditions for Cu(II) and Cd(II) addition (Fig. 3). After the addition of Cu(II) or Cd(II), a large quenching effect was observed for Cu(II), whereas negligible quenching effects were found for Cd(II), indicating effective binding of DOM with Cu(II).[1,42] The quenching characteristics of these components with the addition of Cu(II) and Cd(II) were quite similar to those found for surface water DOM and macrophyte decomposition DOM.[10,38]

To facilitate further information for the complexation between DOM and metals, the logarithmic stability constants (log K_M) and the fraction of the binding fluorophores (f) calculated using the Ryan–Weber model for components and Cu(II) are listed in Table 2. However, the fluorescent quenching curves

fail to fit the experimental data for Cd(II), which may result from the quenching or enhancement of the curve.[10] The log K_M values for all the sampled organic components was found to vary over a wide range (4.20–4.57 for C1, 4.45–5.40 for C2, and 3.74–4.76 for C3, respectively). The log K_M value for C1 was higher than that for C2 and C3 at 0 d, indicating that humic-like components for DOM exhibited a higher binding affinity than the protein-like counterparts. Furthermore, the log K_M values for C1 under both drying and wetting conditions were lower than that at 0 d, suggesting that the stability constants between Cu(II) with humic-like substance decreased under both drying and wetting conditions.[43] However, the log K_M values for C2 under both drying and wetting conditions were higher than that at 0 d, indicating that the protein-like components of DOM exhibited a high binding affinity under drying/wetting conditions. More-over, the log K_M value for C2 under drying conditions was higher than that under wetting conditions (5.40 > 5.27). The f values for C1 under both drying and wetting were higher than that at 0 days and reached their highest values under wetting
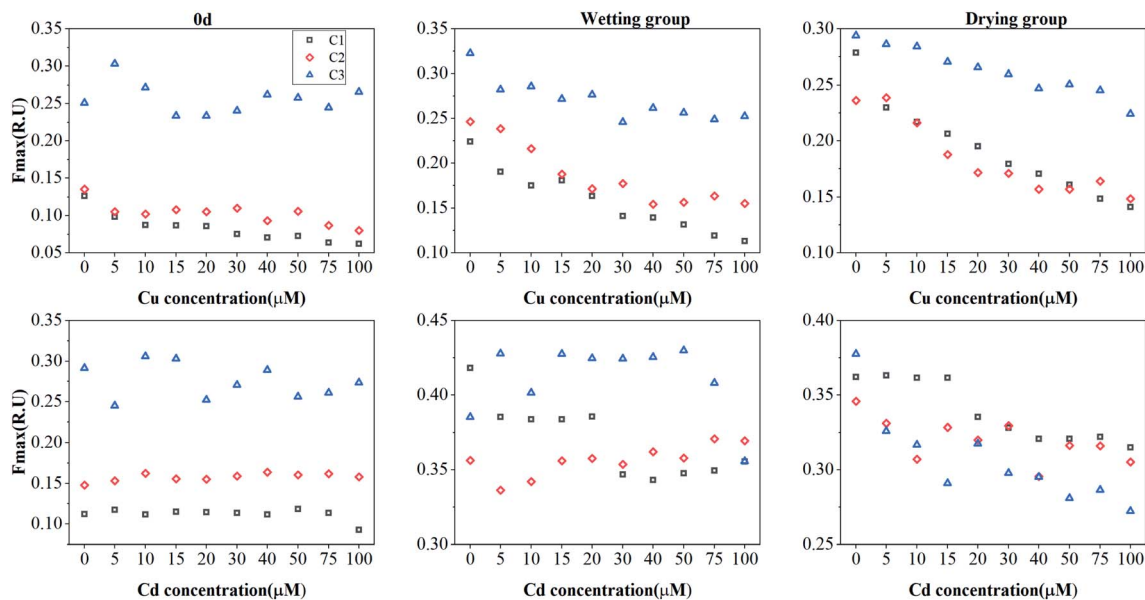
Fig. 3 Change in the F_{max} of PARAFAC-derived three components (C1: humic-like component; C2: tryptophan-like component; C3: tyrosine-like component) with the addition of Cu(II) or Cd(II).

conditions. The f values for C2 under both drying and wetting were found to be lower than that at 0 d, which then reached their lowest values under drying conditions. These results suggest that the Cu(II) binding capacities towards humic-like substances were increased, especially under wetting conditions; in particular, the Cu(II) binding capacities towards protein-like substances decreased under drying conditions.

Compared with Cu(II), Cd(II) addition showed quenching or enhancement, which cannot be successfully fitted by the 1 : 1 complexation model. This may be attributed to the fact that fluorescent substances are enhanced by the complexation of metal ions, as the addition of heavy metals can stimulate some chromophores, especially in the case of Cd(II).[10] Some heavy metals can increase the fluorescence intensity of DOM or produce a competition effect with metal ions.[44]

In summary, the stability constants between Cu(II) and humic-like substances decreased; however, the Cu(II) binding capacities of the component increased under drying/wetting conditions. The Cu(II) affinities and binding capacities towards protein-like substances showed variation under drying/wetting conditions, which may be ascribed to the changes in the

existing pattern of tryptophan-like and tyrosine-like substances in aerobic environments. Our observations are consistent with that of He *et al.*,[40] who characterized the heavy metal binding with DOM from composted municipal solid waste.

3.3 Interaction features between heavy metals and sediment DOM by 2D-SFS-COS

To further describe the binding heterogeneities and degree of preferential binding of sediment DOM with Cu(II) and Cd(II) under both drying and wetting conditions, 2D-SFS-COS was applied to explore the variation among the different peaks (Fig. 4). For Cu(II), in synchronous maps, one positive auto-peak at 280 nm and one cross-peak in the wavelength range of 300–380 nm was observed at 0 d for the wetting group; meanwhile, two positive auto-peaks at 280 nm and 338 nm and one cross-peak in the wavelength range of 300–380 nm were observed for the drying group (Fig. 4a, c and e). This shows that protein-like fluorescence is more susceptible to changes in the concentration of Cu(II). The synchronous maps showed only one positive cross-peak in the wavelength range of 250–280/280 nm, and one negative peak in the wavelength range 280/300–338 nm

Table 2 log K_M and f values for the three components with Cu(II) determined by Ryan and Weber model in sediment-derived DOM at 0 d and 90 d after incaution under drying and wetting conditions

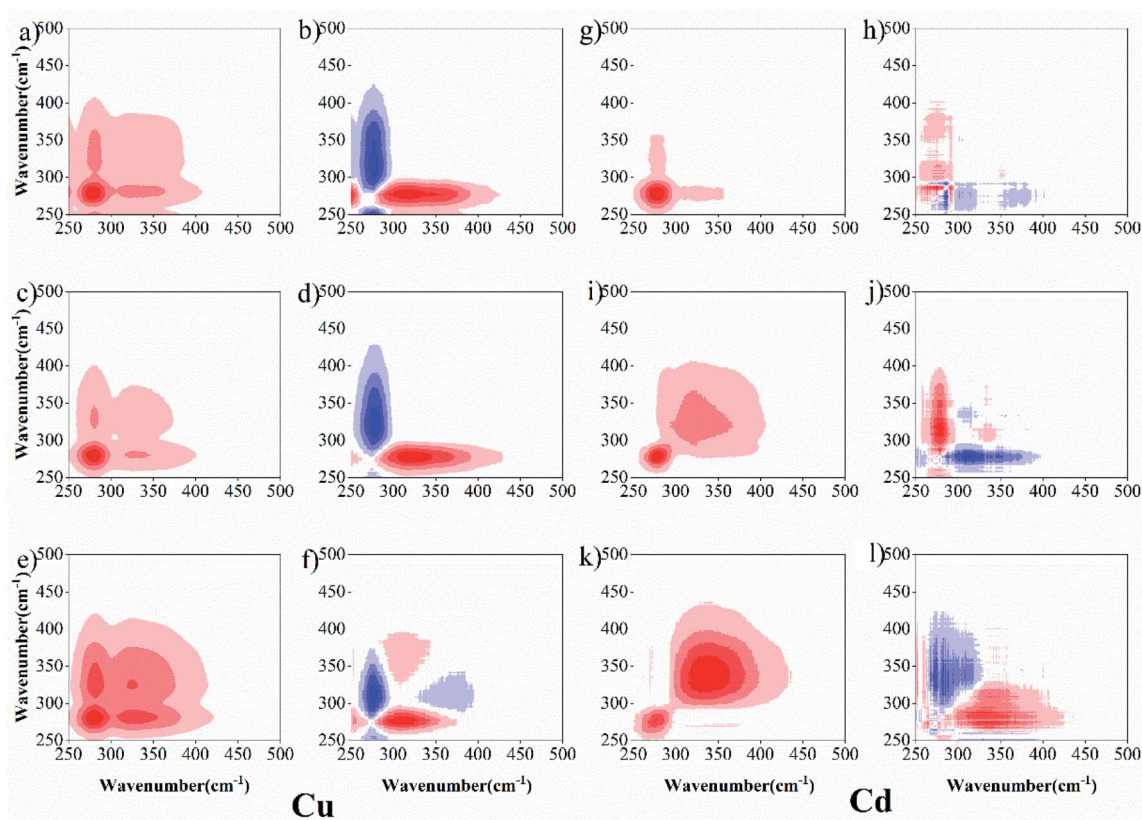| Samples	C1			C2			C3		
	log K_M	f	r^2	log K_M	f	r^2	log K_M	f	r^2
0 d	4.57	61.8	0.98	4.45	45.1	0.66	FM[a]	—	—
Drying group	4.24	70.8	0.99	5.40	41.2	0.92	3.74	49.1	0.95
Wetting group	4.20	74.2	0.97	5.27	44.8	0.94	4.79	26.3	0.88

[a] FM: failure model.

Fig. 4 Synchronous and asynchronous 2DCOS maps of synchronous fluorescent spectra (SFS) of derived DOM with titrated Cu at 0 d (a and b), for wetting group (c and d) and for drying group (e and f) and of derived DOM with titrated Cd at 0 d (g and h), for wetting group (i and j), and for drying group (k and l). Red represents positive correlations, and blue represents negative correlations with higher color intensity indicating a stronger positive or negative correlation.

at 0 d for the wetting group, respectively (Fig. 4b and d). Two positive auto-peaks at 280 nm and 380 nm and one negative cross-peak at 338 nm were detected below the diagonal line in the asynchronous map for the drying group (Fig. 4f). According to the Noda rule,[27] the sequence of reactions is as follows: 250–280 → 300–338 nm at 0 d for the wetting group; 280 → 380 → 338 nm for the drying group. The wavelength ranges of 250–300 nm, 300–380 nm, and 380–550 nm can be roughly assigned to the protein-like, fulvic-like, and humic-like fluorescence fractions, respectively.[5] These results suggest that the binding ability of DOM towards Cu(II) ions follows the order of protein-like → humic-like at 0 d for the wetting group and protein-like → humic-like → fulvic-like for the drying group. Protein-like substances were more dominant in the DOM–Cu(II) interaction process, similar to that found by Guo et al.,[14] who used Fourier-transform infrared, UV-Vis and fluorescence spectra combined with two-dimensional correlation to clarify the binding properties of copper and lead onto compost-derived DOM. In addition, according to the report of Gou et al.,[14] the intensities for the auto-peaks can be ordered as follows: wetting group (Corr. = 110 310.605) > drying group (Corr. = 38 516.222) > 0 d (Corr. = 12 051.175) at 280 nm to the synchronous maps. This suggested that the degree of preferential binding was enhanced under wetting conditions. From the above, DOM

under drying conditions with Cu(II) has more binding sites, which may be attributed to the fact that higher aromatic, hydrophobic, and molecular weight fractions were observed in sediment DOM under drying conditions. Whereas DOM under wetting conditions with Cu(II) shows a higher degree of preferential binding.

For Cd (Fig. 4g, i and k), two positive auto-peaks were observed at 276 nm and 350 nm for the synchronous 0 d drying group, and one positive auto-peak was observed at 276 nm for the synchronous wetting group. The asynchronous maps (Fig. 4h, j and l) show only one positive cross-peak in the wavelength range 276/300–350 nm for 0 d, and one negative peak in the wavelength range 300–350/276 nm was identified for both drying and wetting groups, respectively. These results suggest that the binding ability of DOM toward Cd(II) ions follows the order: fulvic-like → protein-like for 0 d and protein-like → fulvic-like for drying and wetting groups. Meanwhile, the intensities for the auto-peaks can be ordered as follows: wetting group (Corr. = 47 745.877) > drying group (Corr. = 17 904.4) > 0 d (Corr. = 867.655) at 276 nm to the synchronous maps. These results also suggest that the drying/wetting conditions influence the heterogeneous distribution and binding affinities of the binding sites between DOM–Cu(II) and DOM–Cd(II).

3.4 Interaction features between heavy metals and sediment DOM by 2D-FTIR-COS

2D-FTIR-COS analysis was used to investigate the differences in DOM binding sites with Cu(II) and Cd(II) under drying/wetting conditions. The synchronous and asynchronous maps for DOM binding with metals ranged from 1800 cm^{-1} to 900 cm^{-1}.[45,46] For Cu(II) (Fig. 5), the synchronous map for 0 d includes three positive auto-peaks, with one peak at 1625 cm^{-1} and the other two peaks at 1380 cm^{-1} and 1138 cm^{-1}, respectively (Fig. 5a). According to previous studies, the band at approximately 1625 cm^{-1} can be ascribed to aromatic C=C,[14] the peak at 1380 cm^{-1} corresponds to the OH deformation of the phenolic hydroxyl group,[47] and the peak at

1138 cm^{-1} is related to C–O stretching for alcohols, ethers, and esters.[48] All cross-peaks in the synchronous maps were positive, indicating that the signals for the functional groups simultaneously changed with metal concentration. Two positive cross-peaks (1625/1138 cm^{-1}, 1380/1138 cm^{-1}) were observed, and one negative cross-peak (1625/1380 cm^{-1}) was observed for the Cu(II) addition (Fig. 5b). According to the Noda rule,[27] the sequence of the binding affinities for Cu(II) for 0 d followed the order: 1380 cm^{-1} > 1625 cm^{-1} > 1138 cm^{-1}. Therefore, it can be concluded that phenol–OH has a stronger affinity towards Cu(II) than the N–H of the amide group or C–O group at 0 d.

Six positive auto-peaks were observed at 1705 cm^{-1}, 1450 cm^{-1}, 1190 cm^{-1}, and 1072 cm^{-1} for the wetting group (Fig. 5c), and six auto-peaks were observed at 1680 cm^{-1},
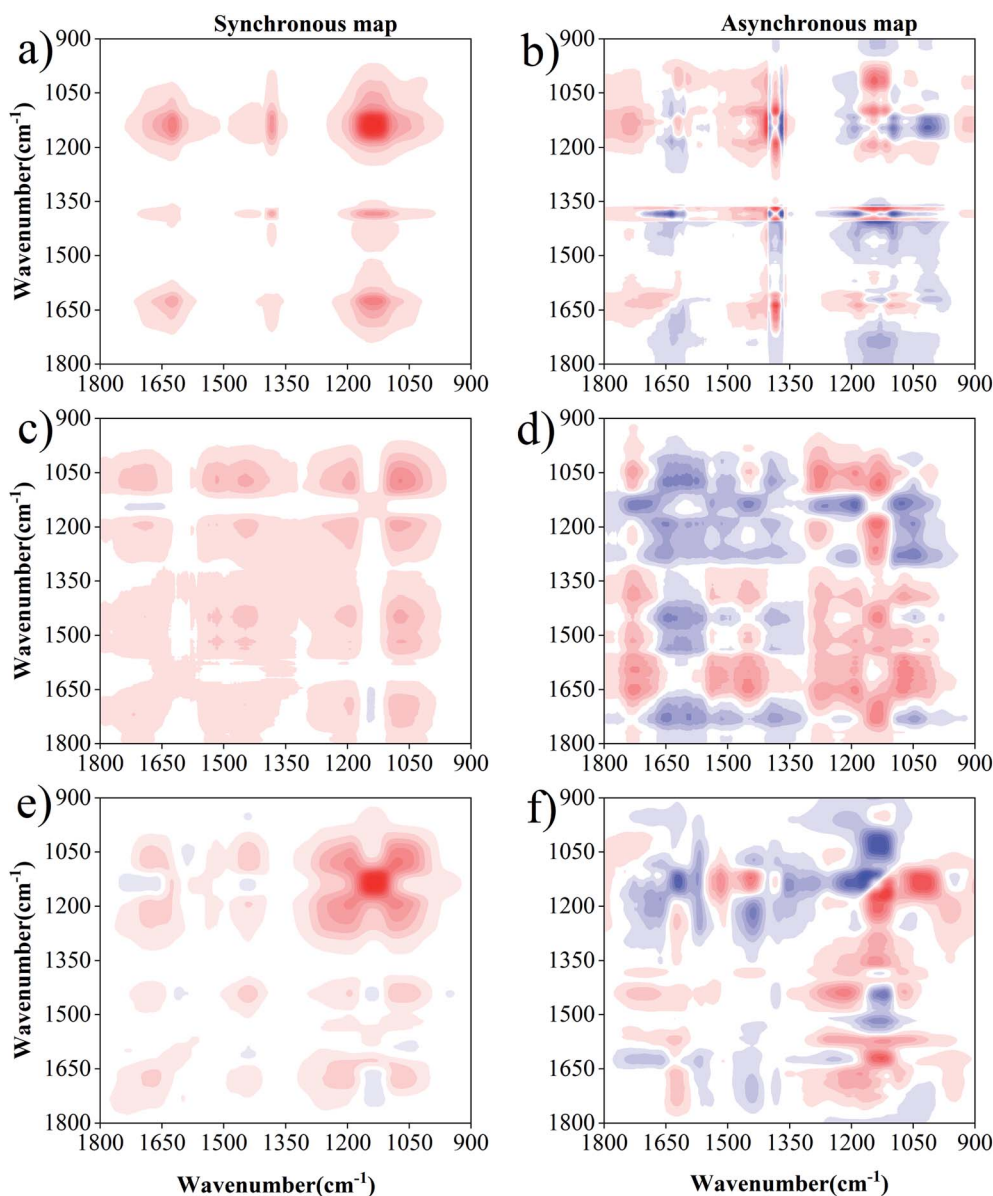

Fig. 5   Synchronous and asynchronous 2DCOS maps of Fourier-transform infrared (FTIR) spectra of derived DOM with titrated Cu at 0 d (a and b), for wetting group (c and d) and for drying group (e and f). Red represents positive correlations, and blue represents negative correlations with higher color intensity indicating a stronger positive or negative correlation.

Fig. 6 Synchronous and asynchronous 2DCOS maps of Fourier-transform infrared (FTIR) spectra of derived DOM with titrated Cd at 0 d (a and b), for wetting group (c and d) and for drying group (e and f). Red represents positive correlations, and blue represents negative correlations with higher color intensity indicating a stronger positive or negative correlation.
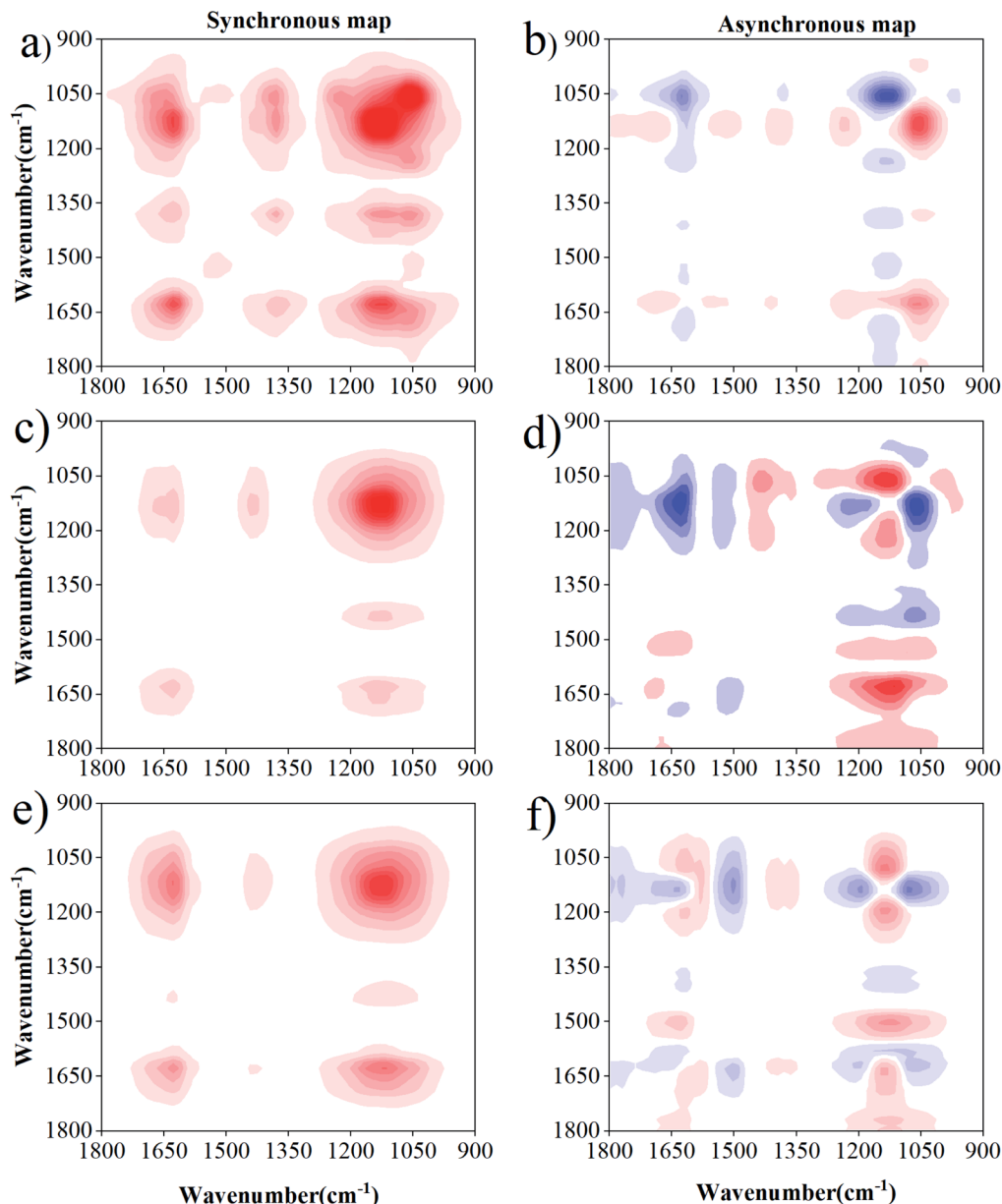
1520 cm^{-1}, 1438 cm^{-1}, 1190 cm^{-1}, 1130 cm^{-1}, and 1078 cm^{-1} for the drying group (Fig. 5e). In combination with the asynchronous maps (Fig. 5b and f), the sequence for the binding affinity of Cu(II) for the wetting group followed the order: 1705 > 1190 > 1450 > 1072. Meanwhile, the sequence of the binding affinity of Cu(II) for the drying group followed the order: 1190 > 1680 > 1438 > 1078 > 1138 > 1520. The peaks at 1705 cm^{-1}, 1680 cm^{-1}, 1520 cm^{-1}, 1450–1438 cm^{-1}, 1190 cm^{-1}, 1138 cm^{-1}, and 1078–1072 cm^{-1} correspond to carboxylic acid, amide, aromatic, aliphatic, phenol, carbohydrate, and ester, respectively.[5,9,48,49] The change in the functional groups of DOM upon binding with Cu(II) under wetting conditions followed the sequence of carboxyl → carbohydrate → aliphatic → ester.

Under wetting conditions, carboxyl was the most sensitive group towards Cu(II) addition. This is consistent with previous reports, which demonstrate that the carboxyl in DOM accounts for a high Cu(II) binding ability.[43,50] Meanwhile, the sequence of functional group change under drying conditions followed the order of phenolic → amide → aliphatic → ester → carbohydrate → aromatic. Phenolic was the most sensitive group towards Cu(II) addition, in which the abundance of phenols was enriched with the increasing degree of humification under drying conditions (higher aromaticity existed in drying group). This result is similar to the complexation of heavy metals to hyperthermophilic compost – derived HA and thermophilic compost – derived HA.[50] Contrary to the lack of observation at

0 d, polysaccharides and carboxyl groups were observed under both drying and wetting conditions. However, aromatic and amide groups were not observed in the wetting group, and carboxylic acid was not observed in the drying group. This result seems to complement and confirm the observations from the UV-Vis spectra that higher aromaticity is observed in DOM under drying conditions. In addition, differences exist in the binding sites and sequences for DOM with Cu under wetting conditions, which may be due to the anaerobic decomposition of protein-like substances.[32] Meanwhile, the preferential binding sequence with the functional groups was also different under drying/wetting conditions. These results provide great insight underlying the differences in the binding properties produced by structural changes in DOM under different moisture conditions, which is in agreement with the study of Hur et al.[51]

The 2D-FTIR-COS analysis for DOM–Cd(ɪɪ) is shown in Fig. 6. The synchronous maps for DOM–Cd(ɪɪ) are very similar to the results obtained for DOM–Cu(ɪɪ) at 0 d. The sequence of the binding affinities for Cd(ɪɪ) for 0 d followed the order of phenol > amide > carbohydrate. Differences were observed in the susceptibility and binding sites between the drying group and wetting group with Cd(ɪɪ). The most susceptible functional groups for Cd(ɪɪ) binding were characterized by bands located at 1138 cm^{-1} and 1640 cm^{-1} for the drying group and wetting group, respectively (Fig. 6b and c). A negative peak at 1138 cm^{-1} and 1640 cm^{-1} was observed in the drying group and wetting group, respectively (Fig. 6e and f). The DOM functional groups under drying/wetting conditions with Cd(ɪɪ) followed the sequence of carbohydrate → amide. The binding affinities for DOM with Cd decreased under drying and wetting conditions. Besides, the three positive peaks at 1705 cm^{-1}, 1520 cm^{-1}, 1450 cm^{-1}, and 1078 cm^{-1} were not observed in DOM–Cd(ɪɪ), showing that more binding sites and higher binding affinities exist for DOM with Cu(ɪɪ) than that with Cd(ɪɪ). Such different sequences between Cu(ɪɪ) and Cd(ɪɪ) can be likely attributed to their particular chemical properties.[52] The results show fewer binding sites and lower binding affinities for DOM with Cd(ɪɪ) than with Cu(ɪɪ), especially under drying conditions. The mobility and toxicity of heavy metals may be reduced after binding with inorganic or organic ligands, according to the study of Sheng et al.[23] and Huang et al.[53] Thus, Cd(ɪɪ) may show a high environmental hazard due its relatively low binding capabilities and binding stability. Meanwhile, heavy metals with DOM under wetting conditions are more likely to migrate and transform owing to the action of water flow.

4 Conclusion

In this research, structural changes and complexation of sediment DOM with Cu and Cd under drying/wetting conditions were investigated by multi-spectroscopic methods. Strong aromatic and hydrophobic and high molecular weight substances were observed in DOM under drying conditions. In addition, humic-like and protein-like components were mainly found in bottomland sediment. EEM-PARAFAC modeling suggested that the stability constants for Cu(ɪɪ) with humic-like

substances decreased; however, the binding capacities for Cu(ɪɪ) with the component were found to increase under drying and wetting conditions. 2DCOS-SFS-COS and 2D-FTIR-COS analyses showed that the drying and wetting conditions influenced the heterogeneous distribution and binding affinities for the binding sites between DOM–Cu(ɪɪ) and DOM–Cd(ɪɪ). In general, the binding stability and binding abilities for Cu(ɪɪ) with DOM are higher than those for Cd(ɪɪ) under drying and wetting conditions. Fewer binding sites exist for Cu(ɪɪ) and Cd(ɪɪ) with DOM under wetting conditions than under drying conditions. Therefore, drying/wetting conditions may play an important role in determining the environmental risk and bioavailability for heavy metals. The effect of drying/wetting conditions on the environmental behavior of heavy metals in bottomland sediment should not be overlooked.

Conflicts of interest

There are no conflicts to declare.

References

1 H. Xu, L. Zou, D. Guan, W. Li and H. Jiang, Molecular weight-dependent spectral and metal binding properties of sediment dissolved organic matter from different origins, *Sci. Total Environ.*, 2019, **665**, 828–835.

2 B. Huang, *et al.*, Adsorption characteristics of Cu and Zn onto various size fractions of aggregates from red paddy soil, *J. Hazard. Mater.*, 2014, **264**, 176–183.

3 H. Xu, G. Yu, L. Yang and H. Jiang, Combination of two-dimensional correlation spectroscopy and parallel factor analysis to characterize the binding of heavy metals with DOM in lake sediments, *J. Hazard. Mater.*, 2013, **263**(Pt 2), 412–421.

4 M. Chen and J. Hur, Pre-treatments, characteristics, and biogeochemical dynamics of dissolved organic matter in sediments: a review, *Water Res.*, 2015, **79**, 10–25.

5 W. Chen, N. Habibul, X. Y. Liu, G. P. Sheng and H. Q. Yu, FTIR and synchronous fluorescence heterospectral two-dimensional correlation analyses on the binding characteristics of copper onto dissolved organic matter, *Environ. Sci. Technol.*, 2015, **49**, 2052–2058.

6 M. Pesaro, G. Nicollier, J. Zeyer and F. Widmer, Impact of soil drying-rewetting stress on microbial communities and activities and on degradation of two crop protection products, *Appl. Environ. Microbiol.*, 2004, **70**, 2577–2587.

7 Z. Li, *et al.*, Spectroscopic study of the effects of dissolved organic matter compositional changes on availability of cadmium in paddy soil under different water management practices, *Chemosphere*, 2019, **225**, 414–423.

8 J. D. Hosen, O. T. McDonough, C. M. Febria and M. A. Palmer, Dissolved Organic Matter Quality and Bioavailability Changes Across an Urbanization Gradient in Headwater Streams, *Environ. Sci. Technol.*, 2014, **48**, 7817–7824.

9 M. Huang, *et al.*, Investigating binding characteristics of cadmium and copper to DOM derived from compost and

rice straw using EEM-PARAFAC combined with two-dimensional FTIR correlation analyses, *J. Hazard. Mater.*, 2018, **344**, 539–548.

10 D. H. Yuan, *et al.*, Detection of copper(II) and cadmium(II) binding to dissolved organic matter from macrophyte decomposition by fluorescence excitation–emission matrix spectra combined with parallel factor analysis, *Environ. Pollut.*, 2015, **204**, 152–160.

11 P. N. Williams, *et al.*, Organic matter–solid phase interactions are critical for predicting arsenic release and plant uptake in Bangladesh paddy soils, *Environ. Sci. Technol.*, 2011, **45**, 6080–6087.

12 M. Zhang, L. Cui, L. Sheng and Y. Wang, Distribution and enrichment of heavy metals among sediments, water body and plants in Hengshuihu Wetland of Northern China, *Ecol. Eng.*, 2009, **35**, 563–569.

13 Z. H. Shao, P. J. He, D. Q. Zhang and L. M. Shao, Characterization of water-extractable organic matter during the biostabilization of municipal solid waste, *J. Hazard. Mater.*, 2009, **164**, 1191–1197.

14 X. J. Guo, X. S. He, C. W. Li and N. X. Li, The binding properties of copper and lead onto compost-derived DOM using Fourier-transform infrared, UV-Vis and fluorescence spectra combined with two-dimensional correlation analysis, *J. Hazard. Mater.*, 2019, **365**, 457–466.

15 B. Hu, *et al.*, Investigating spectroscopic and copper-binding characteristics of organic matter derived from sediments and suspended particles using EEM-PARAFAC combined with two-dimensional fluorescence/FTIR correlation analyses, *Chemosphere*, 2019, **219**, 45–53.

16 J. Wen, *et al.*, The complexation of rhizosphere and nonrhizosphere soil organic matter with chromium: using elemental analysis combined with FTIR spectroscopy, *Ecotoxicol. Environ. Saf.*, 2018, **154**, 52–58.

17 X. J. Guo, D. H. Yuan, J. Y. Jiang, H. Zhang and Y. Deng, Detection of dissolved organic matter in saline-alkali soils using synchronous fluorescence spectroscopy and principal component analysis, *Spectrochim. Acta, Part A*, 2013, **104**, 280–286.

18 N. Muhammad, *et al.*, Changes in microbial community structure due to biochars generated from different feedstocks and their relationships with soil chemical properties, *Geoderma*, 2014, **226–227**, 270–278.

19 G. H. Yu, *et al.*, Binding of organic ligands with Al(III) in dissolved organic matter from soil: implications for soil organic carbon storage, *Environ. Sci. Technol.*, 2012, **46**, 6102–6109.

20 T. Jiang, *et al.*, Influence of dissolved organic matter (DOM) characteristics on dissolved mercury (Hg) species composition in sediment porewater of lakes from southwest China, *Water Res.*, 2018, **146**, 146–158.

21 J. Dilling and K. Kaiser, Estimation of the hydrophobic fraction of dissolved organic matter in water samples using UV photometry, *Water Res.*, 2002, **36**, 5037–5044.

22 J. R. Helms, A. Stubbins, J. D. Ritchie and E. C. Minor, Absorption spectral slopes and slope ratios as indicators of molecular weight, source, and photobleaching of chromophoric dissolved organic matter, *Limnol. Oceanogr.*, 2008, **53**, 955–969.

23 G. P. Sheng, *et al.*, Thermodynamic analysis on the binding of heavy metals onto extracellular polymeric substances (EPS) of activated sludge, *Water Res.*, 2013, **47**, 607–614.

24 D. K. Ryan and J. H. Weber, Fluorescence quenching titration for determination of complexing capacities and stability constants of fulvic acid, *Anal. Chem.*, 1982, **54**, 986–990.

25 M. Bahram, R. Bro, C. Stedmon and A. Afkhami, Handling of Rayleigh and Raman scatter for PARAFAC modeling of fluorescence data using interpolation, *J. Chemom.*, 2006, **20**, 99–105.

26 C. A. Stedmon and R. Bro, Characterizing dissolved organic matter fluorescence with parallel factor analysis: a tutorial, *Limnol. Oceanogr.: Methods*, 2008, 572–579.

27 I. Noda and Y. Ozaki, *Two-dimensional correlation spectroscopy: applications in vibrational and optical spectroscopy*, John Wiley & Sons, 2005.

28 J. Wen, *et al.*, Binding characteristics of cadmium and zinc onto soil organic matter in different water managements and rhizosphere environments, *Ecotoxicol. Environ. Saf.*, 2019, **184**, 109633.

29 K. P. Tsai and A. T. Chow, Growing Algae Alter Spectroscopic Characteristics and Chlorine Reactivity of Dissolved Organic Matter from Thermally-Altered Forest Litters, *Environ. Sci. Technol.*, 2016, **50**, 7991–8000.

30 J. Hur, M. H. Park and M. A. Schlautman, Microbial Transformation of Dissolved Leaf Litter Organic Matter and Its Effects on Selected Organic Matter Operational Descriptors, *Environ. Sci. Technol.*, 2009, **43**, 2315–2321.

31 G. Quan, *et al.*, Effects of laboratory biotic aging on the characteristics of biochar and its water-soluble organic products, *J. Hazard. Mater.*, 2020, **382**, 121071.

32 L. Yang, J. H. Choi and J. Hur, Benthic flux of dissolved organic matter from lake sediment at different redox conditions and the possible effects of biogeochemical processes, *Water Res.*, 2014, **61**, 97–107.

33 Y. Li, L. Zhang, S. Wang, H. Zhao and R. Zhang, Composition, structural characteristics and indication of water quality of dissolved organic matter in Dongting Lake sediments, *Ecol. Eng.*, 2016, **97**, 370–380.

34 M. Huang, *et al.*, Application potential of biochar in environment: insight from degradation of biochar-derived DOM and complexation of DOM with heavy metals, *Sci. Total Environ.*, 2019, **646**, 220–228.

35 C. A. Stedmon, S. Markager and R. Bro, Tracing dissolved organic matter in aquatic environments using a new approach to fluorescence spectroscopy, *Mar. Chem.*, 2003, **82**, 239–254.

36 C. Liu, *et al.*, Characterizing dissolved organic matter in eroded sediments from a loess hilly catchment using fluorescence EEM-PARAFAC and UV-Visible absorption: insights from source identification and carbon cycling, *Geoderma*, 2019, **334**, 37–48.

37 S. K. L. B. Ishii and H. Treavor, Behavior of reoccurring PARAFAC components in fluorescent dissolved organic

matter in natural and engineered systems: a critical review, *Environ. Sci. Technol.*, 2012, **46**, 2006–2017.

38 Y. Yamashita, Assessing the dynamics of dissolved organic matter (DOM) in coastal environments by excitation emission matrix fluorescence and parallel factor analysis (EEM-PARAFAC), *Limnol. Oceanogr.*, 2008, **53**(5), 1900–1908.

39 L. Feng, *et al.*, Chemical Composition of Microbe-Derived Dissolved Organic Matter in Cryoconite in Tibetan Plateau Glaciers: Insights from Fourier Transform Ion Cyclotron Resonance Mass Spectrometry Analysis, *Environ. Sci. Technol.*, 2016, **50**, 13215–13223.

40 X. He, *et al.*, Characterizing the heavy metal-complexing potential of fluorescent water-extractable organic matter from composted municipal solid wastes using fluorescence excitation–emission matrix spectra coupled with parallel factor analysis, *Environ. Sci. Pollut. Res.*, 2014, **21**, 7973–7984.

41 C. J. Williams, Y. Yamashita, H. F. Wilson, R. Jaffé and M. A. Xenopoulos, Unraveling the role of land use and microbial activity in shaping dissolved organic matter characteristics in stream ecosystems, *Limnol. Oceanogr.*, 2010, **55**, 1159–1171.

42 W. B. Chen, D. S. Smith and C. Gueguen, Influence of water chemistry and dissolved organic matter (DOM) molecular size on copper and mercury binding determined by multiresponse fluorescence quenching, *Chemosphere*, 2013, **92**, 351–359.

43 X. S. He, *et al.*, Insight into the evolution, redox, and metal binding properties of dissolved organic matter from municipal solid wastes using two-dimensional correlation spectroscopy, *Chemosphere*, 2014, **117**, 701–707.

44 S. E. Cabaniss, Synchronous fluorescence spectra of metal-fulvic acid complexes, *Environ. Sci. Technol.*, 1992, **26**, 1133–1139.

45 H. Xu, L. Guo and H. Jiang, Depth-dependent variations of sedimentary dissolved organic matter composition in a eutrophic lake: implications for lake restoration, *Chemosphere*, 2016, **145**, 551–559.

46 H. A. Abdulla, E. C. Minor and P. G. Hatcher, Using two-dimensional correlations of 13C NMR and FTIR to investigate changes in the chemical composition of dissolved organic matter along an estuarine transect, *Environ. Sci. Technol.*, 2010, **44**, 8044–8049.

47 S. Xue, Q. L. Zhao, L. L. Wei and N. Q. Ren, Behavior and characteristics of dissolved organic matter during column studies of soil aquifer treatment, *Water Res.*, 2009, **43**, 499–507.

48 E. Smidt and K. Meissl, The applicability of Fourier transform infrared (FT-IR) spectroscopy in waste management, *J. Waste Manage.*, 2007, **27**, 268–276.

49 H. A. N. Abdulla, E. C. Minor, R. F. Dias and P. G. Hatcher, Changes in the compound classes of dissolved organic matter along an estuarine transect: a study using FTIR and 13C NMR, *Geochim. Cosmochim. Acta*, 2010, **74**, 3815–3838.

50 J. Tang, *et al.*, Insight into complexation of Cu(II) to hyperthermophilic compost-derived humic acids by EEM-PARAFAC combined with heterospectral two dimensional correlation analyses, *Sci. Total Environ.*, 2019, **656**, 29–38.

51 J. Hur and B. M. Lee, Characterization of binding site heterogeneity for copper within dissolved organic matter fractions using two-dimensional correlation fluorescence spectroscopy, *Chemosphere*, 2011, **83**, 1603–1611.

52 W. Li, *et al.*, Composition and copper binding properties of aquatic fulvic acids in eutrophic Taihu Lake, China, *Chemosphere*, 2017, **172**, 496–504.

53 B. Huang, *et al.*, Effects of soil particle size on the adsorption, distribution, and migration behaviors of heavy metal(loid)s in soil: a review, *Environ. Sci.: Processes Impacts*, 2020, **22**, 1596–1615.

54 P. G. Coble, S. A. Greent, N. V. Blought and R. B. Gagosia, Characterization of dissolved organic carbon matter in the Black Sea by fluorescence spectroscopy, *Nature*, 1990, **348**(29), 432–435.